Available online at www.sciencedirect.com
ScienceDirect
Earth and Planetary Science Letters 250 (2006) 89–103
EPSL
www.elsevier.com/locate/epsl

Chemostratigraphy of the Neoproterozoic Mirassol d'Oeste cap dolostones (Mato Grosso, Brazil): An alternative model for Marinoan cap dolostone formation

E. Font [a,b,*], A. Nédélec [b], R.I.F. Trindade [a], M. Macouin [b], A. Charrière [b]

[a] *Instituto de Astronomia, Geofísica e Ciências Atmosféricas, Universidade de São Paulo, São Paulo, Brazil*
[b] *LMTG, UMR #5563, OMP, Université Paul-Sabatier, Toulouse, France*

Received 5 December 2005; received in revised form 2 May 2006; accepted 29 June 2006
Available online 7 September 2006
Editor: V. Courtillot

Abstract

We have conducted a detailed study of the Neoproterozoic Mirassol d'Oeste cap dolostones that overlay the glacial diamictites of the Puga Formation (~635 Ma, Amazon craton, Brazil) in order to understand the formation of these post-glacial dolostones. Petrographic features indicate that the dolostones are primary to early diagenetic in origin and precipitated in a moderately shallow-water platform corresponding to a carbonate ramp during transgressive conditions. Major and trace element contents, as well as C and O isotopic signatures, are consistent with an anoxic sediment influenced by sulphate-reducing bacteria. Such an environment is known to provide favourable conditions for the precipitation of dolomite as observed nowadays in modern hypersaline lagoons. Isotopic compositions of tube-like structures suggest local upward fluid seepage from the underlying cap dolostone. Our data concur with geochemical data from other Neoproterozoic cap dolostones to support a microbially-mediated model in specific environmental conditions for the formation of these unusual deposits worldwide.

Keywords: Neoproterozoic; Marinoan glaciation; Cap dolostone; Sulphate-reducing bacteria; Amazonian craton

1. Introduction and geological setting

The Neoproterozoic era encompasses at least three glacial events (Sturtian, Marinoan and Gaskiers glaciations). The corresponding glacial deposits (diamictites and tillites) are usually overlain by "cap" carbonates composed by a lowermost cap dolostone and an upper (cap) limestone, marking severe climatic changes from icehouse to greenhouse conditions [1]. Paleomagnetic data from Neoproterozoic glacial deposits and associated cap carbonates show that ice caps have extended into equatorial latitudes [2–5], comforting the hypothesis of a Neoproterozoic snowball Earth [6].

Cap carbonates are especially well developed over the Marinoan Neoproterozoic glacial successions (recently dated at ~635 Ma [7]) and give us an insight on environmental changes in this ice-age aftermath. They form transgressive sequences associated to the post-glacial sea-level rise and comprise a thin basal dolomitic unit (the so-called cap dolostones) and a thick overlying cap limestone

* Corresponding author. IAG-USP, Cidade universitária, Rua do Matão, 1226, 05508-090, São Paulo, Brazil. Tel.: +55 11 3091 2790; fax: +55 11 8101 5045.
E-mail addresses: eric@iag.usp.br, font_eric@hotmail.com (E. Font).

0012-821X/$ - see front matter © 2006 Elsevier B.V. All rights reserved.
doi:10.1016/j.epsl.2006.06.047

succession. Stratigraphic and isotopic data of Marinoan cap carbonates, and especially their negative C isotope compositions, have been extensively reported for Australia, Namibia, Canada, China, Svalbard and Amazonia (see summary by [8] and references therein), but are still a matter of debate. In addition, the Marinoan cap dolostones show unusual structures such as tube-like structures, aragonite fans and megaripples (or pseudo-tepees) which received diverse interpretations [1,9].

Recently, the Neoproterozoic cap dolostones of the Mirassol d'Oeste Formation (Mato Grosso, Brazil, Fig. 1), which were deposited above the Puga diamictites in the south-east of the Amazon craton [10], yielded a dual polarity component providing a low paleolatitude for the Amazon craton at the end of the glaciation [4]. The primary character of the magnetization was suggested by the presence of several stratabound geomagnetic reversals and certified by a magnetic mineralogy study that unravelled detrital haematite and detrital magnetite as the remanence carriers [4,11]. Nogueira et al. [12] proposed a post-Marinoan age for the Mirassol d'Oeste (MO) cap dolostones on the basis of C isotopic correlations with the Maieberg and the Elantoek Formations, Namibia. These latter formations that cap the Ghaub glacial deposits have

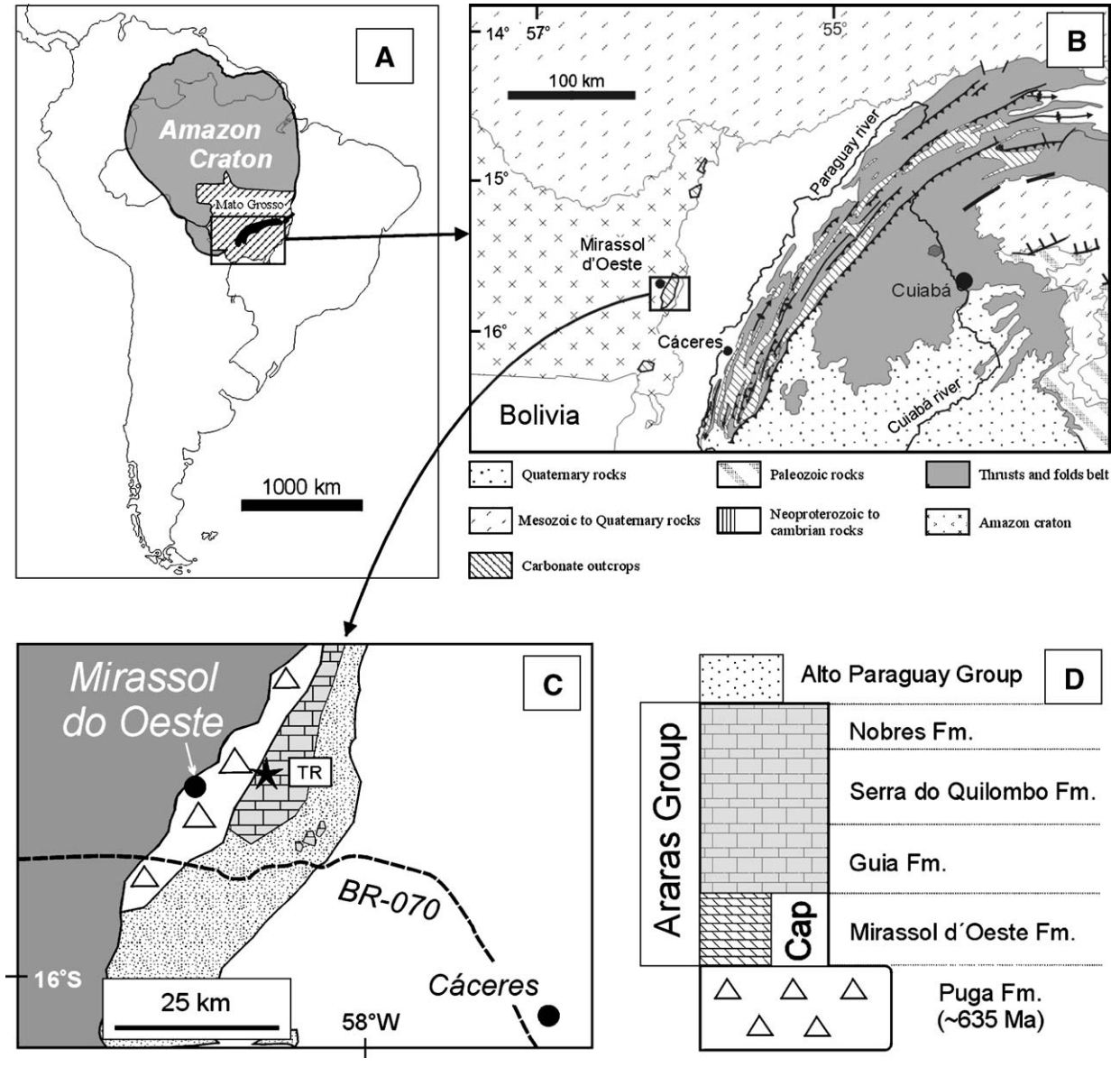

Fig. 1. Location of the Amazon craton (A) and Paraguay belt (B). Geological map of the studied sector (C) with localization of Terconi section (TR) and regional stratigraphic sequence (D).

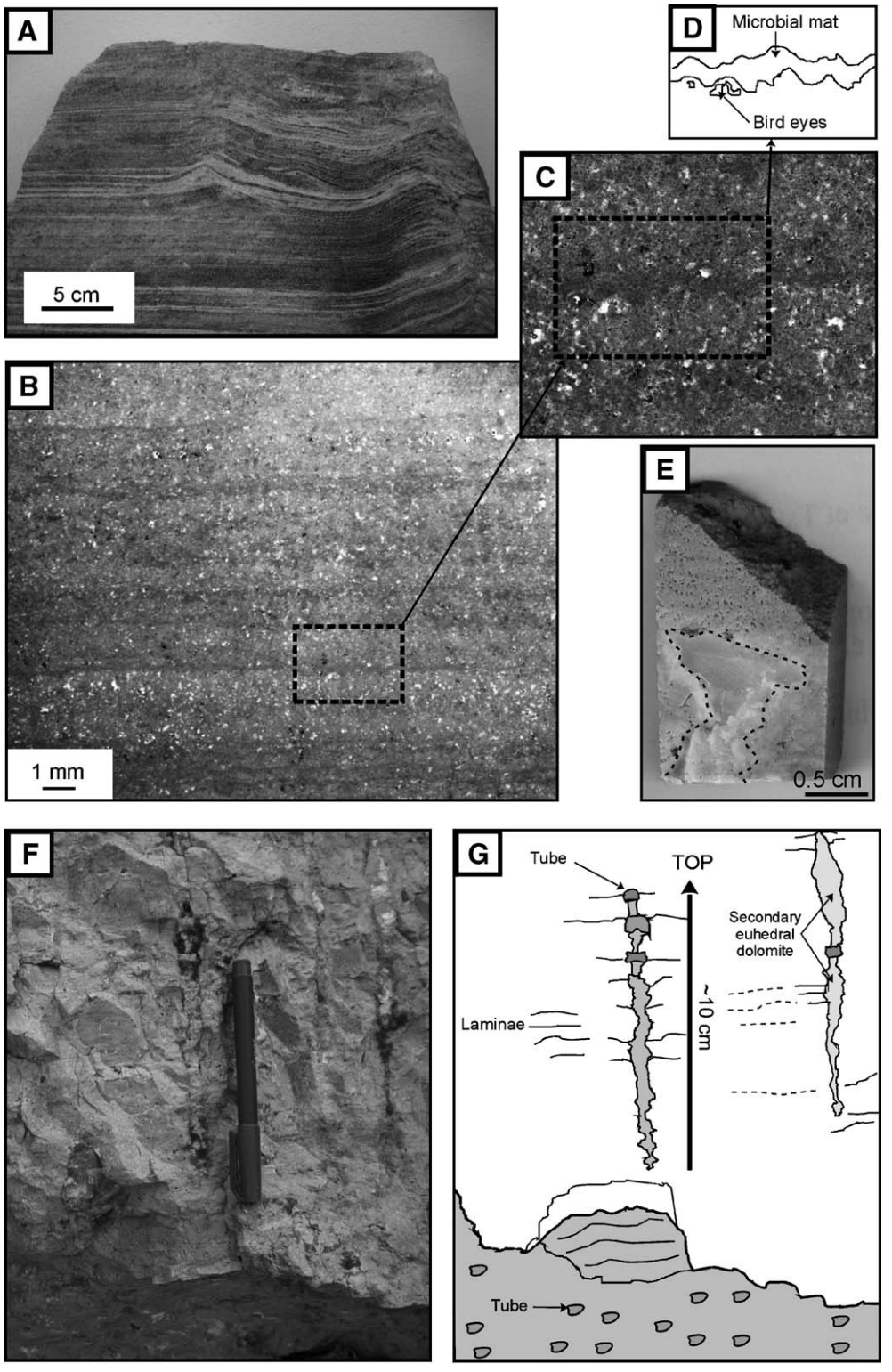

Fig. 2. Macroscopic and microscopic observations of MO dolostones: (A) Wavy stromatolites; (B) sequences showing alternation of micritic layers and dolosparite filled with keystone vugs layers (sample TR 5W); (C) and (D) dark stromatolitic layers and fenestral layers (see wavy stromatolitic structures at the bottom); (E) detail of a tube-like structure bumping into the uppermost laminations; (F) and (G) preserved and recrystallized tube-like structures.

Table 1
Major and trace element contents of the MO dolostones

Samples	TR 1F	TR 2E	TR 3C	TR 4Q	TR 5E	TR 5I	TR 5J	TR 5L	TR 5Q	TR 5W	Mean
SiO2 (%)	0.21	0.53	0.16	0.27	0.49	0.58	0.92	0.47	0.73	1.82	0.62
Al2O3	0.12	0.25	0.08	0.15	0.23	0.30	0.42	0.20	0.30	0.66	0.27
Fe2O3	0.26	0.25	0.27	0.31	0.54	0.52	0.60	0.54	0.50	0.74	0.45
MnO	0.19	0.11	0.15	0.11	0.20	0.19	0.23	0.21	0.20	0.26	0.18
MgO	21.93	21.08	17.25	21.02	19.87	20.56	21.77	20.53	20.94	20.45	20.54
CaO	30.14	31.32	38.01	31.22	31.99	30.21	31.89	30.53	31.03	29.63	31.60
Na2O	<L.D.	<L.D.	<L.D.	<L.D.	<L.D.	<L.D.	<L.D.	<L.D.	<L.D.	<L.D.	
K2O	<L.D.	<L.D.	<L.D.	<L.D.	<L.D.	<L.D.	<L.D.	<L.D.	<L.D.	0.06	0.06
TiO2	0.01	0.01	0.01	0.02	0.02	0.01	0.03	0.01	0.02	0.04	0.02
P2O5	<L.D.	0.04	<L.D.	<L.D.	<L.D.	<L.D.	0.03	<L.D.	<L.D.	0.02	0.03
PF	46.46	45.96	44.02	46.19	46.15	46.38	42.78	46.49	45.47	45.81	45.57
Total	99.31	99.54	99.95	99.29	99.48	98.74	98.66	98.99	99.17	99.49	99.26
Mg (poids atom)	13.16	12.65	10.35	12.61	11.92	12.34	13.06	12.32	12.56	12.27	12.32
Mg (nb atom)	0.55	0.53	0.43	0.53	0.50	0.51	0.54	0.51	0.52	0.51	0.51
Ca (poids atom)	21.53	22.37	27.15	22.30	22.85	21.58	22.78	21.81	22.16	21.16	22.57
Ca (nb atom)	0.54	0.56	0.68	0.56	0.57	0.54	0.57	0.55	0.55	0.53	0.56
Ca/Mg	0.98	1.06	1.57	1.06	1.15	1.05	1.05	1.06	1.06	1.03	1.11
As (ppm)	1.19	1.10	1.48	<L.D.	<L.D.	<L.D.	<L.D.	<L.D.	<L.D.	<L.D.	1.26
Ba	30.40	20.40	33.60	19.05	15.71	16.67	6.67	9.04	10.18	9.26	17.10
Cd	1.94	1.45	1.72	0.54	6.64	4.25	2.71	4.43	2.46	3.21	2.94
Co	2.11	1.78	1.14	0.80	0.86	1.01	1.10	0.90	0.89	1.20	1.18
Cs		<L.D.	<L.D.	0.12	0.18	0.21	0.33	0.18	0.32	0.42	0.25
Cu	9.50	13.40	6.10	5.25	12.01	10.67	21.57	19.47	7.23	7.12	11.23
Ga	0.13	0.25	<L.D.	0.13	0.19	0.24	0.61	0.33	0.30	0.78	0.33
Hf	0.08	0.10	0.27	0.21	0.11	0.09	0.17	0.07	0.11	0.29	0.15
Mo	<L.D.	<L.D.	<L.D.	<L.D.	<L.D.	<L.D.	0.72	0.64	0.82	1.48	0.91
Mn	1471.83	852.11	1161.97	867.61	1526.06	1456.34	1742.96	1657.75	1533.80	1998.59	1426.90
Nb	0.20	0.36	0.13	0.34	0.31	0.30	0.57	0.22	0.38	1.01	0.38
Ni	12.70	15.40	9.90	8.84	6.42	6.56	9.05	6.76	6.35	6.59	8.86
Pb	14.50	15.10	8.09	9.07	147.65	109.27	50.87	125.95	68.67	127.37	67.65
Rb	<L.D.	0.54	<L.D.	0.59	1.13	1.12	1.75	0.95	1.72	2.90	1.34
Sr	43.10	51.60	39.60	45.26	60.12	53.87	52.02	50.79	54.65	59.14	51.02
Ta	0.02	0.03	0.01	0.03	0.03	0.03	0.05	0.02	0.03	0.09	0.03
Th	0.14	0.24	0.09	0.22	0.32	0.32	0.56	0.24	0.41	0.92	0.35
U	1.31	1.15	0.63	0.96	0.69	0.68	0.86	0.53	0.62	1.09	0.85
V	4.60	5.20	4.90	3.75	6.38	5.96	9.55	7.33	6.34	8.55	6.26
W	<L.D.	<L.D.	<L.D.	<L.D.	<L.D.	<L.D.	<L.D.	<L.D.	<L.D.	<L.D.	
Y	0.98	1.37	0.72	1.02	1.07	1.19	1.82	1.45	2.17	2.70	1.45
Zn	36.10	40.20	28.10	16.58	197.00	267.40	546.80	592.20	201.50	144.80	207.07
Zr	4.02	4.63	12.60	9.75	3.95	3.42	6.74	3.14	4.65	10.90	6.38
La (ppm)	0.54	0.80	0.39	0.64	1.20	1.24	1.68	1.32	1.82	2.48	1.21
Ce	1.43	1.70	0.98	1.43	2.33	2.40	3.30	2.76	3.53	4.91	2.48
Pr	0.19	0.24	0.13	0.18	0.29	0.31	0.43	0.35	0.46	0.63	0.32
Nd	0.86	1.03	0.55	0.73	1.08	1.20	1.68	1.34	1.80	2.51	1.28
Sm	0.20	0.23	0.12	0.17	0.22	0.24	0.33	0.28	0.39	0.53	0.27
Eu	0.04	0.05	0.03	0.03	0.05	0.05	0.07	0.06	0.07	0.11	0.06
Gd	0.19	0.23	0.11	0.16	0.18	0.20	0.31	0.24	0.35	0.48	0.24
Tb	0.03	0.03	0.02	0.02	0.03	0.03	0.05	0.04	0.06	0.07	0.04
Dy	0.14	0.19	0.10	0.15	0.17	0.19	0.27	0.22	0.33	0.43	0.22
Y	0.04	0.05	0.03	0.04	0.04	0.04	0.07	0.05	0.08	0.10	0.05
Ho	0.03	0.04	0.02	0.03	0.03	0.04	0.05	0.04	0.06	0.09	0.04
Er	0.07	0.10	0.06	0.08	0.10	0.10	0.15	0.12	0.18	0.24	0.12
Tm	0.01	0.01	0.01	0.01	0.01	0.02	0.02	0.02	0.03	0.04	0.02
Yb	0.06	0.09	0.05	0.08	0.09	0.11	0.15	0.11	0.17	0.25	0.12
Lu	0.01	0.01	0.01	0.01	0.02	0.02	0.02	0.02	0.03	0.04	0.02
C org (%)	0.05	0.04	0.03	0.03	0.04	0.04	0.04	0.11	0.04	0.05	0.05
S tot	<0.01	<0.01	<0.01	<0.01	<0.01	<0.01	<0.01	<0.01	<0.01	<0.01	
Y/Ho	550.93	265.41	809.52	435.08	275.63	211.83	153.79	319.44	222.83	90.74	333.52

Table 1 (*continued*)

Samples	TR 1F	TR 2E	TR 3C	TR 4Q	TR 5E	TR 5I	TR 5J	TR 5L	TR 5Q	TR 5W	Mean
Sum REE	3.80	4.76	2.57	3.71	5.79	6.13	8.51	6.91	9.26	12.79	6.42
NdN/YbN [21]	1.17	0.97	0.87	0.79	0.95	0.95	0.93	0.99	0.89	0.83	0.93
GdN/Gd* [21]	1.17	1.16	1.09	1.11	1.03	1.04	1.12	1.01	1.06	1.10	1.09
PrN/YbN [22]	1.01	0.88	0.77	0.74	0.98	0.95	0.91	0.99	0.87	0.81	0.89
Pr/Pr* [22]	1.01	1.06	1.00	1.02	1.07	1.08	1.07	1.06	1.07	1.06	1.05
Ce/Ce* [22]	1.00	0.88	1.01	0.98	0.91	0.89	0.89	0.93	0.89	0.90	0.93
Eu/Eu* [22]	1.05	1.06	1.13	1.04	1.09	1.09	1.08	1.05	0.96	1.10	1.07
(Sm/Yb)N	1.66	1.33	1.20	1.10	1.16	1.16	1.12	1.28	1.17	1.08	1.22
La_N/Sm_N [23]	0.40	0.50	0.46	0.56	0.81	0.75	0.74	0.68	0.68	0.67	0.63

REE anomalies are calculated following Bau and Duslki [22].

been precisely dated at 635±1,2 Ma (U–Pb zircon method; [13]), consistent with a recent Pb–Pb age yielding a 627±32 Ma age for the MO cap dolostones [14].

Here, we report a petrographic and chemostratigraphic study of the MO cap dolostones including high resolution isotopic compositions, in order to check their origin. In addition and by comparison with cap dolostones elsewhere, this study allows to propose an alternative model for the formation of these enigmatic cap dolostones.

2. Materials and methods

Major and trace elements were analyzed from chemically and thermally untreated bulk samples at the SARM-CNRS laboratory in Nancy. Samples were carefully selected as the best preserved ones by thin section examination. Rock samples were grinded using agate mortar. Major elements were analyzed by ICP-AES with analytical uncertainties generally less than 2%. Trace elements were analyzed by ICP-MS with analytical uncertainties generally less than 10%. The quality of the analyses was checked by comparison with international geostandards.

A set of 69 samples (noted TR) were collected with a sampling spacing of about 20 cm in the 24 m thick cap dolostones, that crop out in the Terconi quarry. These whole rock samples were prepared by sealed tube reactions of the carbonate with 100% phosphoric acid (H_3PO_4) (d>1.92 g/cm^3) at 25 °C. After 12 h, the first gas likely corresponding to the reaction with calcite was eliminated. After 48 h, the resulting CO_2 gas regarded to be derived from the reaction of the phosphoric acid with dolomite was analyzed with a mass spectrometer (GEO 20-20 by EUROPA) at the Instituto de Geociências in São Paulo University. In addition, six small samples were extracted from a larger sample with tube-like structures for local scale isotopic determination. Following the same procedure, these samples, after the release of the first gas, were heated at 80 °C during 2 h to extract the CO_2 from the dolomite. The amount of extracted CO_2 and its carbon and oxygen isotopic compositions were measured using a helium continuous-flow mass spectrometer (AP-2003) at the Institut de Physique du Globe de Paris (IPGP laboratory). Results are calibrated with respect to an internal standard in the laboratory and reported in delta notation (δ) in parts per thousand (‰) relative to PDB standard. The confidence of the measurement is about ±0.2‰.

3. Field and microscopic observations

The Neoproterozoic cap dolostones of the MO Formation are made of pinkish dolomudstone mainly consisting of planar or wavy laminae described in detail by Nogueira et al. [10] (Fig. 2A). Dolomicrite is the principal constituent of the matrix, while dolosparite occurs as secondary mineral filling vugs and microcracks (Fig. 2B). The sediment is characterized by a laminated structure showing alternation of two types of laminae, millimetric in thickness, which are extremely homogeneous along the entire sedimentary column, although not always recognizable with the naked eye (Fig. 2B–C). Layers of compact micrite (≤1 mm thick) containing numerous peloids alternate with layers (1–3 mm in thickness) characterized by a fenestral microstructure with keystone vugs sometimes filled with secondary dolosparite (recrystallized bird eyes), as can be seen in Fig. 2C–D. These primary structures are sometimes modified by styloliths. In several samples, brown wavy laminae are interbedded within the micritic layers and are assigned to stromatolites or mineralized former microbial mats (Fig. 2C–D). From sites TR1 to sites TR2, the low occurrence of keystone vug layers indicates deeper, subtidal conditions. From sites TR3 up to sites TR5, fenestrae frequency increases suggesting shallower conditions. Stromatolites, i.e. former microbial mats wherein minerals were precipitated or localised as a by-product of metabolic activities of microbial communities, are localized in the middle part of the section and are associated with bird eyes structures

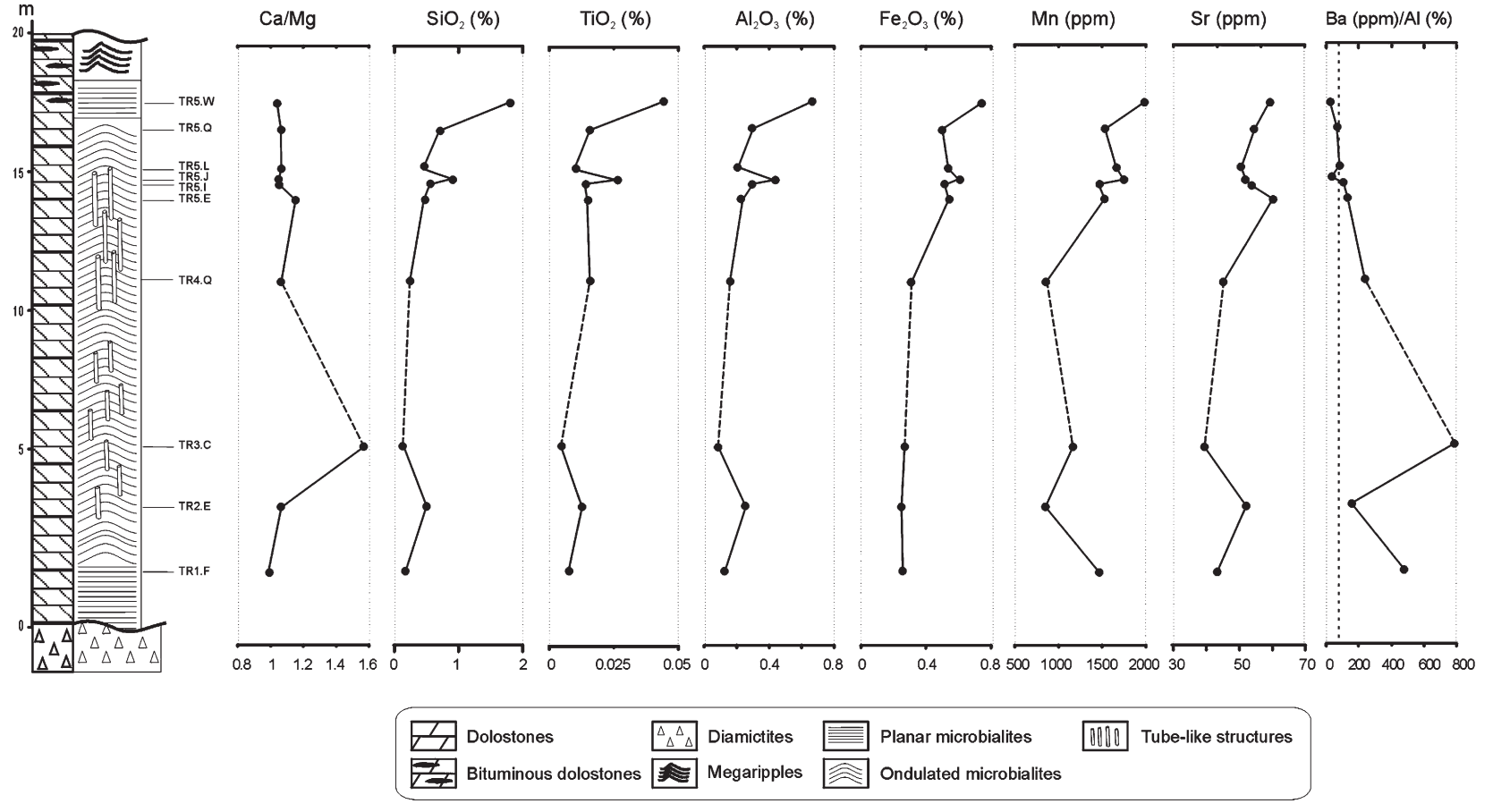

Fig. 3. Vertical distribution of major element contents and some trace element (wt.%) in the Mirassol d'Oeste cap dolostone samples. Dotted vertical line in the Ba profile corresponds to the value of average shale from Wedepohl [29].

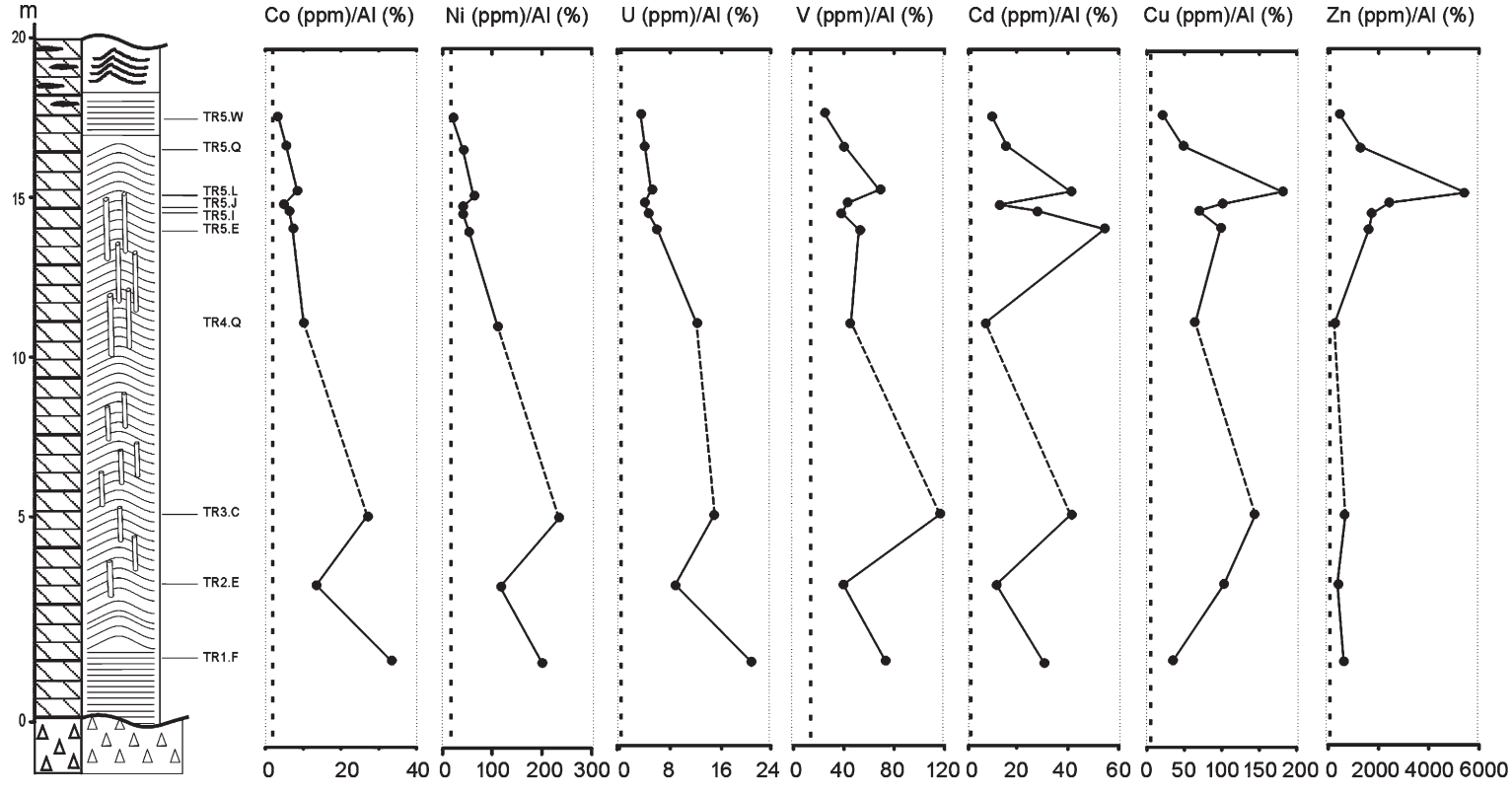

Fig. 4. Vertical distribution of redox-sensitive trace element contents (ppm) normalized by Al (%). Dotted vertical lines correspond to values of average shale from Wedepohl [29].

(Fig. 2C–D). The stromatolites form domal structures of c.a. 1 m in diameter at the base of the sequence and of c.a. 10 cm in diameter at the upper part of the sequence (Fig. 2A). The middle part of the sedimentary column is also characterized by the occurrence of tube-like structures of an unknown origin (Fig. 2E–F–G). These structures have a diameter of <3 cm and locally interrupt and dislocate the microbial lamination. Combined vertical and horizontal sections of tube rocks enable to recognize a complex plumbing network (Fig. 2E). The tubes are filled with pink dolomicrite (or dolosparite) or secondary euhedral dolomite. At the top, the facies change gradually to grey dolostones with abundant organic matter, calcite cements and characteristic megaripples [10]. Most of the dolostone layers are sub-horizontal or slightly dipping (<5°) to the east and are neither deformed (except for some synsedimentary deformation) nor metamorphosed.

4. Chemostratigraphy

4.1. Major elements

Major and trace element contents of the analyzed samples are given in Table 1 and the vertical evolution of major elements is presented in Fig. 3. Whole rock MgO contents (~20–22.5%) and CaO contents (~30–38%) confirm that the dolostones are mainly made of dolomite or Ca-dolomite (Ca/Mg range is 1–1.1 for most samples).

Elements of typical detrital origin have relatively low values (SiO_2, TiO_2, Al_2O_3, Fe_2O_3 <2%) indicating few detrital supply from the continent. In addition, the co-variation of TiO_2 and Al_2O_3 shows that the detrital source did not change during the dolostone deposition. Nevertheless, a global increase of their contents is noted towards the top at the base of the bituminous dolostones, possibly announcing the geochemical and environmental changes at the transition between the dolostones and the limestone sequences. Values of TOC are low (0.03–0.05 wt.%) through most of the section, except in the sample TR 5L (TOC = 0.11 wt.%). S contents are always very low (<0.01 wt.%).

4.2. Trace elements

Mn contents are high and range from 700 to 2000 ppm (Table 1). The highest Mn values are observed at the base and at the top of the section. Sr contents display a narrow variation range from 40 to 60 ppm (Fig. 3). Despite low TOC values, paleoproductivity seems to have been important in the lower half of the section as suggested by the high Ba/Al [15]. Ba/Al decreases to below the shale average in the upper part of the section, whereas immediately above organic carbon is still preserved. Particular attention is given here to chalcophile redox-sensitive elements that can be used to discuss the oxic/anoxic conditions of the sediment at deposition time [16,17]. They are reported as ratios to Al% (or Al ppm $\times 10^{-4}$) in order to check any over-detrital enrichment (Fig. 4). Two groups can be recognised: Co, Ni, U on one side and V, Cd, Cu and Zn on the other side, with diverging evolutions. The first group displays the highest contents toward the base of the section. These elements follow a very similar evolution with decreasing contents from TR4 upwards. These elements can be fixed in high amounts under reducing conditions, either precipitated as sulphides or bound to organic matter [16]. Cu and Zn display a similar evolution with a noticeable enrichment in sample TR 5L, i.e. in the uppermost stromatolites.

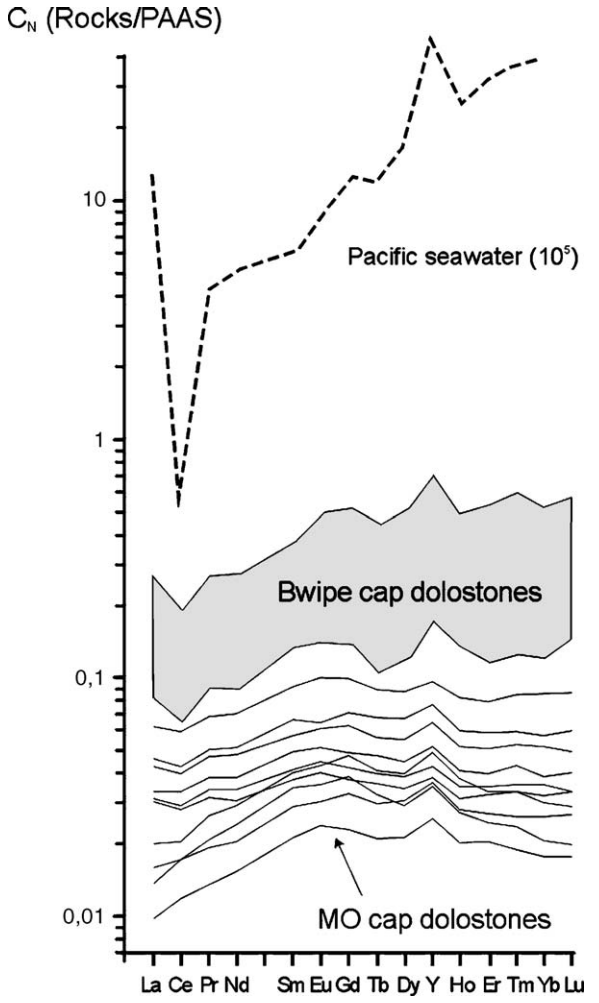

Fig. 5. REE distribution patterns of MO dolostones. REE patterns of the Bwipe dolostones [27] and of the Atlantic seawater [22] are shown for comparison.

High Cd/Al is recorded at different levels in the section; it is an indicator of sulphide production from sulphate reduction, even at a low production level [18]. In this hypothesis, the high Cd contents and the very low concentration of S would indicate that H_2S was lost, possibly due to the lack of available iron inhibiting substantial pyrite formation.

Total REE concentrations of MO dolostones vary from 3 to 13 ppm (Table 1). These values lie within the range of average marine carbonates (0.04–14 ppm; [19]). Webb and Kamber [20] showed that microbialite carbonates incorporate YREE in equilibrium with seawater. Thus, YREE in ancient microbialitic carbonates can be used as palaeoenvironmental proxies [21]. Fig. 5 shows PAAS normalised YREE patterns exhibiting a relative depletion in LREE with respect to HREE (average $[Nd/Yb]_N=0.93$). A small positive Gd anomaly (Gd/Gd^* calculated as $Gd_N/0.33Sm_N+0.67Tb_N$ averages 1.09) is also observed, as well as a noticeable Y/Ho enrichment (average ratio=333) dismissing any significant terrigenous input as well as any secondary dolomitization [21]. All these features are evocative of seawater-like patterns. However, contrary to modern seawater, the REE patterns of our samples do not present any significant Ce negative anomaly (average $Ce/Ce^*=0.93$), but displays a small positive Eu anomaly (average Eu/Eu^* calculated after [22]=1.07). Ce contents could be altered during diagenesis, but Morad and Felitsyn [23] suggest that the Ce anomaly represents a primary signature if there is no correlation between La_N/Sm_N and Ce (with the condition $La_N/Sm_N>0.35$). In the MO dolostones, the La_N/Sm_N ratio is superior to 0.35 for all samples and there is no apparent correlation between La_N/Sm_N and Ce anomaly thus excluding diagenetic influence (Table 1). Therefore, we conclude that the REE patterns of the MO dolostones are primary and reflect the Neoproterozoic post-glacial seawater-composition that impregnated the sediment.

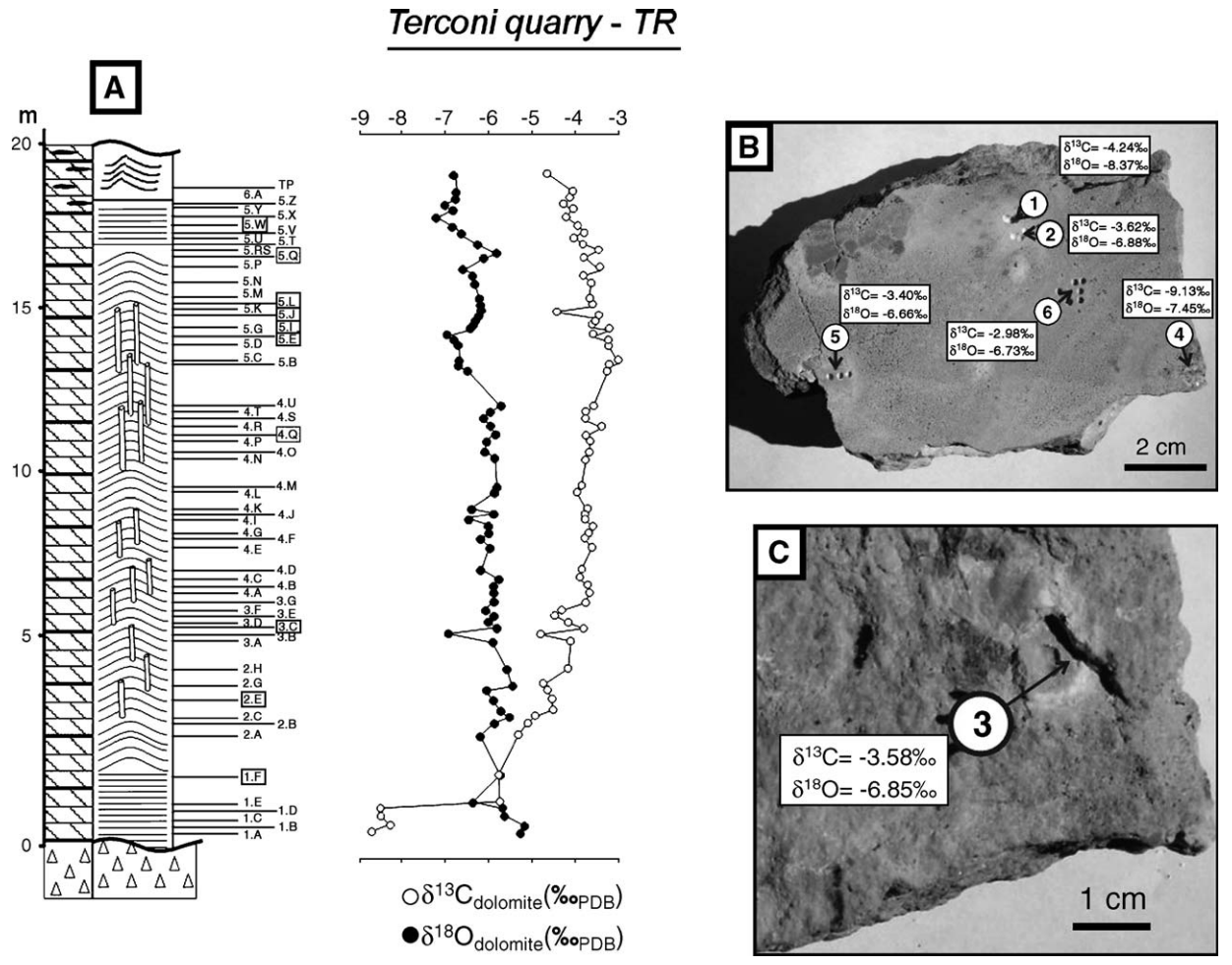

Fig. 6. Detailed isotopic ($C_{dolomite}$ and $O_{dolomite}$) data of Terconi section (TR) and tube-like structures (site TR5).

Table 2
C and O isotopic data

Site	*d* (m)	*d* ^{13}C ‰ (PDB)	*d* ^{18}O ‰ (PDB)
TR 1A	0.13	−8.73	−5.24
TR 1B	0.36	−8.29	−5.15
TR 1C	0.66	−8.48	−5.61
TR 1D	0.86	−8.49	−5.67
TR 1E	1.06	−5.76	−6.34
TR 1F	2.06	−5.76	−5.72
TR 2A	3.36	−5.31	−6.17
TR 2B	3.76	−5.08	−5.86
TR 2C	3.96	−4.93	−5.52
TR 2D	4.16	−4.52	−5.7
TR 2E	4.56	−4.54	−5.88
TR 2F	4.86	−4.65	−6.05
TR 2G	5.06	−4.73	−5.42
TR 2H	5.56	−4.22	−5.55
TR 3A	6.46	−4.1	−5.88
TR 3B	6.71	−4.8	−6.92
TR 3C	6.91	−3.81	−5.82
TR 3D	7.11	−4.18	−5.99
TR 3E	7.31	−4.48	−5.88
TR 3F	7.51	−4.33	−5.84
TR 3G	7.81	−3.75	−6.06
TR 4A	8.06	−3.67	−5.85
TR 4B	8.31	−3.71	−5.87
TR 4C	8.56	−3.9	−5.77
TR 4D	8.81	−3.87	−6.14
TR 4E	9.61	−3.62	−5.96
TR 4F	9.91	−3.78	−6.14
TR 4G	10.11	−3.72	−5.97
TR 4H	10.31	−3.61	−5.97
TR 4I	10.51	−3.78	−6.48
TR 4J	10.71	−3.78	−5.85
TR 4K	10.91	−3.74	−6.41
TR 4L	11.41	−3.97	−5.81
TR 4M	11.66	−3.86	−5.79
TR 4N	12.56	−3.76	−5.82
TR 4O	12.81	−3.69	−6.06
TR 4P	13.11	−3.66	−6.04
TR 4Q	13.36	−3.73	−5.84
TR 4R	13.56	−3.39	−5.95
TR 4S	13.86	−3.76	−6.14
TR 4T	14.11	−3.75	−5.91
TR 4U	14.36	−3.57	−5.7
TR 5A	16.00	−3.26	−6.47
TR 5B	16.2	−3.23	−6.67
TR 5C	16.35	−3	−6.63
TR 5D	16.85	−3.23	−6.66
TR 5E	17.05	−3.25	−6.73
TR 5F	17.23	−3.6	−6.9
TR 5G	17.43	−3.22	−6.39
TR 5H	17.63	−3.62	−6.34
TR 5I	17.83	−3.53	−6.29
TR 5J	18.03	−3.46	−6.25
TR 5K	18.23	−4.5	−6.11
TR 5L	18.43	−3.6	−6.18
TR 5M	18.63	−3.67	−6.18
TR 5N	19.08	−3.64	−6.29
TR 5O	19.28	−3.8	−6.32
TR 5P	19.48	−3.42	−6.53
TR 5Q	19.93	−3.8	−6.09
TR 5R 5S	20.13	−3.45	−5.72
TR 5T	20.33	−3.84	−6.23
TR 5U	20.56	−4.03	−6.94
TR 5V	20.79	−3.8	−6.62
TR 5W	20.99	−3.95	−6.73
TR 5X	21.19	−4.21	−7.19
TR 5Y	21.52	−4.08	−6.84
TR 5Z	21.67	−4.27	−6.99
TR 6A	21.87	−4.13	−6.73
TR TP	23.07	−4.71	−6.84
Tubes 1 (tube)		−4.24	−8.37
Tubes 2 (white ring)		−3.62	−6.88
Tubes 3 (Tube)		−3.58	−6.85
Tubes 4 (Tube with recrystallisation)		−9.13	−7.45
Tubes 5 (Tube)		−3.4	−6.66

4.3. C and O isotopes

Some recent studies establish the C and O isotopic signature for the Marinoan-age cap carbonates of the Amazonian craton in Brazil [10,12,24]. However, none of these studies address in detail the basal dolostones of the Araras Group. Instead, they are regional studies, dealing with the whole carbonate succession. We present here a new and very detailed isotopic data set focussed on the cap dolostones.

C and especially O isotopic compositions are sensible to post-depositional diagenetic alteration processes and are used to check the primary nature of isotopic signatures. Alteration due to recrystallization of ancient carbonates in the presence of metamorphic or meteoric fluids is usually denoted by large depletions of ^{18}O in measured samples (e.g. [25]). However, the oxygen isotopic composition of terminal Proterozoic ocean water is not known with great certainty. All δ^{18}O values obtained from the Terconi quarry section are between −5.1 to −7.2‰. The δ^{18}O curve presents oscillating values, but a global trend from the base (maximum value of −5.2‰) to the top of the sequence (minimum value of −7.2‰) is significant (Fig. 6). Excursions are limited in number and size (≤1‰ in absolute values). Besides, δ^{13}C values vary gradually, but rather independently of ^{18}O along the entire section. These results comfort the fact that late fluid-rock interactions were small to negligible.

Like all Neoproterozoic cap dolostones, the Mirassol d'Oeste Formation has negative δ^{13}C values. They range from −8.7‰ to −3.0‰ with significant oscillations observed in the high-resolution sampling

performed here (Fig. 6). Basal dolostones (site TR1) exhibit the most negative values between −8.2‰ and −8.7‰. Upsection, the values rise to −5.7‰ in site TR 1E and then to −3.8‰ (site TR 3G). From site TR 3G to site TR 4U, values are steady between −3.5‰ and −3.7‰. At the upper part of the unit, a small and gradual decrease from around −3 to −4.5‰ is noted towards the contact with bituminous dolostones and the overlying limestones of the Guia Formation.

Isotopic compositions of tube-like structures are given in Table 2. Measurements were done at several points of the sample as illustrated by Fig. 6: into a tube (point 1, 3, 4 and 5), at the contact between a tube and the matrix (point 2), which is characterized by a pale ring bordering the tube, and in the matrix (point 6). Tubes 1, 3 and 5 are filled with pink dolomicrite whereas tube 4 is filled with secondary carbonate (essentially represented by large euhedral dolomite crystals) (Fig. 6). $\delta^{18}O$ values inside the tube are slightly more negative than in the corresponding whole rock sample, but remain in the −6.7 to −8.4‰ range. The most negative $\delta^{18}O$ value is observed in the tube 4 filled with euhedral dolomite in agreement with their obvious secondary nature. For the pink dolomicrite tubes and their rings, $\delta^{13}C$ values range from −3.4‰ to −4.2‰ and are similar to the sample matrix (Fig. 6). The $\delta^{13}C$ value of the tube 4, filled with large secondary dolomite, exhibits a noticeably lower negative value of −9.1‰.

5. Discussion

5.1. Formation and depositional environment of the MO cap dolostones

The geochemical data presented here gives us an insight into the formation mode of the MO dolostones as well as the seawater chemistry of their depositional environment.

The dolomite is suggested to be primary (i.e. penecontemporaneous of deposition) to early diagenetic owing to the preservation of original petrographic structures (laminations, pelletoids and vugs) and to the dolomicritic nature of the matrix.

$\delta^{18}O$ values are in the −5 to −7‰ range, i.e. consistent with the range of early Phanerozoic values and likely to be primary [25]. Veizer et al. [26] recognized a general decreasing trend from 0 (present mean value) to −8‰ in Cambrian times regarded as resulting from an early diagenetic stabilization of metastable carbonate polymorphs, rather than witnessing an increased seawater temperature through time. Hence, we thought that the MO dolostone oxygen isotope signature is not an altered signal and may even record a progressive temperature and/or salinity change during their depositional time. Besides, the MO dolostones show YREE patterns with a sea-water like distribution supporting their unmodified nature.

The sedimentary features of the MO dolostones point to deposition in low energy conditions, at least for most of the section situated under the tepee level. Palaeoenvironmental conditions under which thrive the stromatolite-forming cyanobacteria are restricted to the photic zone, likely in protected sedimentation places where microbial mats can easily develop. Nogueira et al. [10] suggested that the MO dolostones were deposited on a moderately deep platform below the storm-wave base. By contrast, a peritidal setting was proposed for the Neoproterozoic Ghana cap dolostones, where emersion features were locally recognized [27]. This latter case could be similar to the development of protected shallow water coastal settings (embayements, lagoons and sabkhas) that has been recognized in the Persian Gulf in response to the last Quaternary interglacial sea-level rise [28]. Otherwise, because of the large post-Marinoan transgression due to continental ice thaw, extensive carbonate ramps were likely to develop in many places and may have provided a convenient deposition setting for the whole Araras Group.

Anoxic to suboxic conditions at deposition time are identified by paleoredox trace elements proxies. In order to appreciate their relative (over-detrital) enrichment, trace element contents were normalized by Al (%) as illustrated by Fig. 4. In Fig. 7, over-detrital enrichment factors (EF) were determined by comparing these ratios to those of normal shales using data from Wedepohl [29]. This approach has been used by several authors to evaluate trace-element enrichments in modern and ancient sediments [16]. After calculating a mean composition for the entire dolomitic sequence and the enrichment factor in relation to average shales, we compare our data to those of well-known organic matter-rich sediments, such as the Mediterranean sapropels [16] and the Cenomanian–Turonian Boundary Event (CTBE) Black Shales [30] (Fig. 7). The enrichment of redox sensitive elements in the MO dolostones is comparable, and even superior, for Cd, Cu, Ni and Zn, to these two organic-rich cases, and witness dysoxic or anoxic conditions, also consistent with high primary Mn contents. In addition, we suggest that the different variations of the previously recognized two groups of trace metals may be consequent to high but variable sulfidic contents in the post-Marinoan seawater. Indeed, Saito et al. [31] pointed out that, in sulfidic seawater, the relative availability of Ni and Co would have been much larger than that of Cd, Zn and Cu as soon as dissolved HS^- reaches an elevated amount, due to

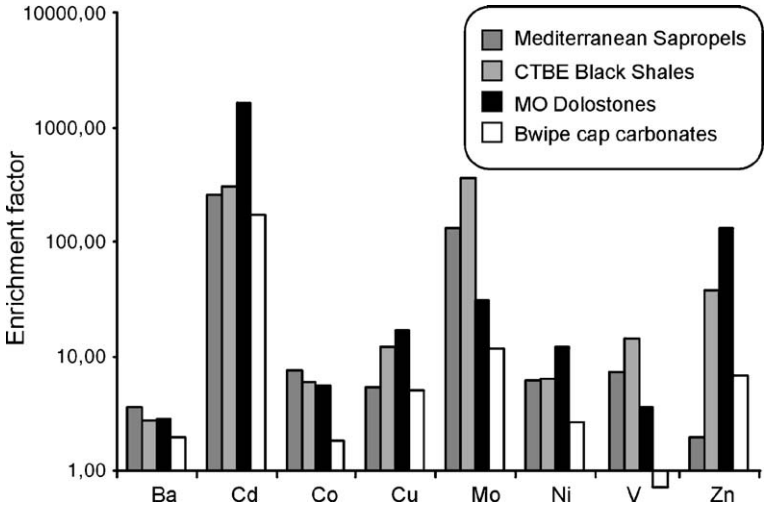

Fig. 7. Enrichment factor of some trace elements of the MO dolostones (in relation to average shales, Wedepohl [29]) compared to Mediterranean sapropels [16], CTBE black shales [30] and Ghana cap dolostones [27].

formation of aqueous sulfide complexes replacing the free ionic species of the latter trace metal group. Besides, the YREE patterns characterized by a very small negative Ce anomaly and a positive Eu anomaly also suggest anoxia, at least at the base of the water-column.

Ba enrichment ratios in MO dolostones are very similar to the selected reference cases pointing to an initially high organic matter content despite the presently rather low TOC (Table 1). The organic matter may have migrated or be degraded in the sediment and the trace element contents alone record its existence, as in the case of some ghost sapropels [16]. Therefore, it is concluded that anoxic conditions and rather high organic matter content prevailed, near the water sediment interface during the formation of the MO cap dolostones.

5.2. A microbially-mediated model for the MO cap dolostones

Bacterial metabolism may aid dolomite precipitation in settings where sulphate-reducing species flourish. Such a scenario is observable nowadays in the hypersaline lagoon of Lagoa Vermelha (Rio de Janeiro, Brazil) and was reproduced in culture experiments [32,33]. In the Neoproterozoic MO dolostones, reducing-sulphates bacteria were probably ubiquitous as indicated by the especially high enrichment factor in Cd [34] (Fig. 7). In these conditions, organic matter (OM) is degraded by the sulphate-reducing bacteria yielding light carbon enriched bicarbonate by the reaction:

$$2(^{12}\mathrm{CHOH})_{\mathrm{OM}} + \mathrm{SO_4^{-2}} \rightarrow \mathrm{H_2S} + 2\mathrm{H}^{12}\mathrm{CO_3^-}$$

Such a microbially mediated model with acting sulphate-reducing bacteria has already been proposed for Ghana cap dolostones by Nédélec et al. [27]. It is also consistent in our case, because of the anoxic to suboxic and organic matter-rich conditions identified by geochemical proxies in the sediment. As no pyrite was formed in the sediments, bacterially generated sulphide are supposed to have exceeded the amount of available iron and H_2S is suggested to have been reoxidized in the water column or liberated in the air [34]. Discharge of H_2S in the air or utilization by anoxygenic sulfide phototrophic bacteria would have favoured solid carbonate precipitation due to increased pH, a necessary condition after Castanier et al. [35]. In addition, sulphate reduction destroys the magnesium–sulphate ion pair, yielding free Mg^{2+} available for the precipitation of early dolomite. Such a metabolic overcoming of the usual inhibitors of dolomite formation was already suggested by Wright [36] for the hypersaline Coorong lakes of South Australia, where dolomite formation occurs presently.

The sulphate reduction reaction described above can be responsible for ^{12}C enrichment of the dissolved bicarbonate and carbonate ions in seawater, providing an explanation for the negative $\delta^{13}C$ observed in the precipitated solid carbonate. Indeed, recent dolostones formed within the sulphate reduction zone always display negative $\delta^{13}C$ values [37].

A microbial origin for the tube-like structures observed in many post-Marinoan cap dolostones is suggested by some authors while others prefer to consider a gas (i.e. methane) escape mechanism [1,38–40]. Evidence of local methane escape has been found by Jiang et al. [38] in the

Doushantuo cap dolostone, where C isotopic compositions locally exhibit strongly negative values ranging from around −10‰ to lower than −40‰, measured on clotted microcrystalline limestone, whereas $\delta^{13}C$ values from the dolomicritic matrix of these rocks are around −3.5‰. These observations are evidence that destabilization of methane hydrates or any methane escape was but a very local and minor process in the post-glacial platforms. On the other hand, Corsetti and Grotzinger [39] have recently described the tube-like structures of the Noonday dolomite (Death Valley, United States) and interpreted them as an upward-propagating microbialite with contemporaneous fill. Here, we have checked for the C and O isotopic composition of the MO dolostones tube-like structures in order to investigate these hypotheses. An upward fluid seepage origin for the tube-like structures of the Mirassol d'Oeste cap dolostones is the most convenient interpretation for the observed fine-scale petrographic structures (Fig. 2). The $\delta^{13}C$ values (Table 2) from the tubes filled with pink dolomicrite are similar to those of the dolomicritic matrix of the sediment in most cases, suggesting that this signature was representative of the seawater chemistry. This is also consistent with a nearly coeval tube and matrix formation, a short time after sedimentation. In one tube, a more negative C-value has been obtained from a secondary dolosparite infilling; hence local influence of a hydrocarbon fluid derived from organic matter burial cannot be excluded, but remains insignificant.

5.3. A uniform model for the all Marinoan cap dolostones?

Neoproterozoic cap carbonates worldwide share several sedimentological features such as fine laminations, tube-like structures, megaripples and a negative $\delta^{13}C$ signature which lead to the interpretation that they were deposited in a common and global depositional environment [1], which remains a matter of debate. The cap dolostones form the transgressive system tracts of the cap carbonate sequences associated with the global post-glacial sea-level rise. Hence, they witness the conditions having prevailed over the resulting large shelf areas. The trace element data imply that the base of the water column that flooded platforms and ramps remained suboxic to anoxic and sulfidic during the deposition of the cap dolostones. Besides, the significance of the negative carbon isotope signature can still be discussed. Our model points to the major influence of bacterial sulfate reduction. Nevertheless, the rather homogeneous nature of the isotopic signal suggests a well-mixed ionic bicarbonate reservoir that is difficult to reconcile with local effects at the water-sediment interface. Recently, Shen et al. [41] unravelled a C-isotopic gradient from −3‰ to −9‰ along a transect from the shelf to the basin in the post-Marinoan deposits of China. They propose that it reflects a vertical gradient in seawater that was maintained because of a sluggish vertical circulation, the deeper water reservoir being the more enriched in light carbon exported from the superficial high productivity zone. Their interpretation agrees with the so-called "turn-over model" of Grotzinger and Knoll [42], i.e. upwelling of a stratified depleted ocean water, as well as with the oxidation of dissolved organic matter in (*deep ?*) ocean water suggested by Rothman et al. [43]. The turnover model is attractive because it is consistent with carbonate precipitation in shallow water conditions with light $\delta^{13}C$ values. Furthermore, it could supply considerable quantity of nutrients and reduced trace metals to the shallow water platform and favour both microbial development and anoxia at the base of the water column. The main problem remaining with such hypotheses is to sustain the upwelling of deep water for all the duration of the cap dolostone formation, i.e. hundreds of thousand years [4]. Although we do not dismiss that the negative C-isotope signature may have a broad scale origin, we stress that it is still consistent with the existence of active sulfate reduction at water-sediment interface, as well as with our model of microbially induced dolomite formation in platform areas.

According to the snowball Earth hypothesis [1], the negative $\delta^{13}C$ values are related to huge swings in atmospheric pCO_2 due to the icehouse/greenhouse global change. However, Halverson et al. [8] pointed that the negative isotopic shift associated with Marinoan cap carbonates actually began before the glaciation. Hence a direct causative link with the post-snowball atmospheric conditions can be questioned and an oceanic cause *sensu lato* is preferred.

6. Conclusions

Our petrographic, geochemical and isotopic data all match a primary to early diagenetic dolomite precipitation mode in the Mirassol d'Oeste cap dolostones. Petrographic features witness the development of microbial mats in a rather protected platform environment. Trace element data show that sedimentation occurred in dysoxic to anoxic conditions, dominated by active sulphate reduction of organic matter. On the basis of a previously recognized modern analog (Lagoa Vermelha, Brazil), we propose that dolomite precipitation at the water-sediment interface or in the uppermost sediment has been mediated by sulphate-reducing bacteria due to anoxia. Isotopic data from tube-like structures show that methane escape was insignificant. Our conclusions are

very similar to those derived from the Neoproterozoic Bwipe cap dolostones of Ghana and might be applied to other cap dolostones worldwide. The reduction of organic matter produced light-carbon enriched bicarbonate ions in seawater, likely contributing to the negative carbon signature of the cap dolostones. However, the global nature of this isotopic signal may also be due to stratified oceanic conditions, responsible for the delivery of anoxic waters of deep origin during the glacio-eustatic flooding of the continental shelf. Transgressive anoxia may explain the carbon isotope signal, but the mediation of the sulphate-reducing bacteria is requested to form the cap dolostones.

Acknowledgments

This research was supported by the Brazilian FAPESP (grants 98/03621-4, 02/02762-0), the French CNRS program ECLIPSE and the CAPES-COFECUB cooperation program (442/4). We thank the contribution of the UFR-SVT of Université Paul Sabatier for a financial ATUPS support. We acknowledge A. Nogueira for his precious help in the stratigraphic control of the sampling. Technical assistance by E. Sampaio and N. Vassard is greatly acknowledged.

References

[1] P.F. Hoffman, D.P. Schrag, The snowball Earth hypothesis: testing the limits of global change, Terra Nova 14 (2002) 129–155.
[2] J.K. Park, Paleomagnetic evidence for low-latitude glaciation during deposition of the Neoproterozoic Rapitan Group, Mackenzie Mountains, N.W.T., Canada, Can. J. Earth Sci. 34 (1997) 34–49.
[3] L.E. Sohl, N. Christie-Blick, D.V. Kent, Paleomagnetic polarity reversals in Marinoan (ca. 600 Ma) glacial deposits of Australia: implications for the duration of low-latitude glaciation in Neoproterozoic time, GSA Bull. 111 (8) (1999) 1120–1139.
[4] R.I.F. Trindade, E. Font, M.S. D'Agrella-Filho, A.C.R. Nogueira, C. Riccomini, Low-latitude and multiple geomagnetic reversals in the Neoproterozoic Puga cap carbonates, Terra Nova 15 (2003) 441–446.
[5] M. Macouin, J. Besse, M. Ader, S. Gilder, Z. Yang, Z. Sun, P. Agrinier, Combined paleomagnetic and isotopic data from the Doushantuo carbonates, South China: implications for the "snowball Earth" hypothesis, Earth Planet. Sci. Lett. 224 (2004) 387–398.
[6] J.L. Kirshvink, Late Proterozoic low-latitude global glaciation: the snowball Earth, in: J.W. Schopf, C. Klein (Eds.), The Proterozoic Biosphere, Cambridge University Press, 1992, pp. 51–52.
[7] D. Condon, M. Zhu, S. Bowring, Y. Jin, W. Wang, A. Yang, From the Marinoan glaciation to the oldest bilaterians: U–Pb ages from the Doushantou Formation, China, Science 308 (2005) 95–98.
[8] G.P. Halverson, P. Hoffman, D. Schrag, A. Maloof, A. Rice, Toward a Neoproterozoic composite carbon isotope record, Geol. Soc. Amer. Bull. 117 (2005) 1181–1207.
[9] N.P. James, G.M. Narbone, T.K. Kyser, Late Neoproterozoic cap carbonates: Mackenzie mountains, northwestern Canada: precipitation and global glacial meltdown, Can. J. Earth Sci. 38 (2001) 1229–1262.
[10] A.C.R. Nogueira, C. Riccomini, A.N. Sial, C.A.V. Moura, T.R. Fairchild, Soft-sediment deformation at the base of the Neoproterozoic Puga cap carbonate (southwestern Amazon Craton, Brazil): confirmation of rapid icehouse–greenhouse transition in snowball Earth, Geology 31 (2003) 613–616.
[11] E. Font, R.I.F. Trindade, A. Nedelec, Detrital Remanence Magnetization in Hematite-bearing Neoproterozoic Puga Cap Dolostone, Amazon Craton: a Rock Magnetic and SEM Study, Geophys. J. Int. 163 (2005) 491–500.
[12] A.C.R. Nogueira, C. Riccomini, A.N. Sial, C.A.V. Moura, R. I. F Trindade, T. R. Fairchild, S and Sr isotope fluctuations and paleoceanographic changes in the late Neoproterozoic Araras carbonate platform, southern Amazon craton, Brazil, Chem. Geol. (in press).
[13] K. Hoffmann, D. Condon, S. Bowring, J. Crowley, A U–Pb zircon date from the Neoproterozoic Ghaub Formation, Namibia: constraints on Marinoan glaciation, Geology 32–9 (2004) 817–820.
[14] M. Babinski, R.I.F. Trindade, J.C. Alvarenga, P.C. Boggiani, D. Liu, Geochronological constraints on Neoproterozoic glaciations in Brazil, Snowball Earth Conf. Ascona (submitted for publication).
[15] W.E. Dean, J.V. Gardner, D.Z. Piper, Inorganic geochemical indicators of glacial-interglacial changes in productivity and anoxia on the California continental margin, Geochim. Cosmochim. Acta 21 (1997) 4507–4518.
[16] B. Warning, H.J. Brumsack, Trace metal signatures of eastern Mediterranean sapropels, Palaeogeogr. Palaeoclimatol. Palaeoecol. 158 (2000) 293–309.
[17] A. Sarkar, S. Sarangi, M. Ebihara, S.K. Bhattacharya, A.K. Ray, Carbonate geochemistry across the Eocene/Oligocene boundary of Kutch, western India: implications to oceanic O2-poor condition and foraminiferal extinction, Chem. Geol. 201 (2003) 281–293.
[18] G. Chaillou, P. Anschutz, G. Lavaux, J. Schäfer, The distribution of Mo, U and Cd in relation to major redox species in muddy sediments of the Bay of Biscay, Mar. Chem. 80 (2002) 41–59.
[19] S.R. Taylor, S.M. McLennan, The Continental Crust: Its Composition and Evolution, Blackwell, Oxford, 1985. 312 pp.
[20] G.E. Webb, B.S. Kamber, Rare earth elements in Holocene reefal microbialites: a new shallow seawater proxy, Geochim. Cosmochim. Acta 64 (2000) 1557–1565.
[21] L.D. Nothdurft, G.E. Webb, B.S. Kamber, Rare earth element geochemistry of Late Devonian reefal carbonates, Canning Basin, Western Australia: confirmation of a seawater REE proxy in ancient limestones, Geochim. Cosmochim. Acta 68 (2004) 263–283.
[22] M. Bau, P. Dulski, Distribution of yttrium and rare-earth elements in the Penge and Kuruman iron-formations, Transvaal Supergroup, South Africa, Precambrian Res. 79 (1996) 37–55.
[23] S. Morad, S. Felitsyn, Identification of primary Ce-anomaly signatures in fossil biogenic apatite: implication for the Cambrian oceanic anoxia and phosphogenesis, Sediment. Geol. 143 (2001) 259–264.
[24] C.J.S. Alvarenga, R.V. Santos, E.L. Dantas, C–O–Sr isotopic stratigraphy of cap carbonates overlying Marinoan-age glacial diamictites in the Paraguay Belt, Brazil, Precambrian Res. 131 (2004) 1–21.
[25] S.B. Jacobsen, A.J. Kaufman, The Sr, C and O isotopic evolution of Neoproterozoic seawater, Chem. Geol. 161 (1999) 37–57.
[26] J. Veizer, D. Ala, K. Azmy, P. Bruckschen, D. Buhl, F. Bruhn, G.A.F. Carden, D. Diener, S. Ebneth, Y. Godderis, T. Jasper, C. Korte, F. Pawellek, O.G. Podlaha, H. Strauss, $^{87}Sr/^{86}Sr$, $\delta^{13}C$ and

$\delta^{18}O$ evolution of Phanerozoic seawater, Chem. Geol. 161 (1999) 225–242.
[27] A. Nédélec, P. Affaton, C. France-Lanord, A. Charrière, J. Alvaro, Sedimentology and chemostratigraphy of the Bwipe Neoproterozoic cap dolostones (Ghana, Volta Basin): a record of microbial activity in a peritidal environment, C.R. Geoscience (2006) doi:10.1016/j.crte.
[28] A. Al-Farraj, An evolutionary model for sabkha development on the north coast of the UAE, J. Arid Environ. 63 (2005) 740–755.
[29] K.H. Wedepohl, The composition of the upper Earth's crust and the natural cycles of selected metals, in: E. Merian (Ed.), Metals and Their Compounds in the Environment, 1991, pp. 3–17.
[30] M.A. Arthur, H.J. Brumsack, H.C. Jenkyns, S.O. Schlanger, Stratigraphy, geochemistry, and paleoceanography of organic carbon-rich Cretaceous sequences, in: R.N. Ginsburg, B. Beauoin (Eds.), Cretaceous Resources, Events and Rhythms, Kluwer, Dordrecht, 1990, pp. 75–119.
[31] M.A. Saito, D.M. Sigman, F.M.M. Morel, The bioinorganic chemistry of the ancient ocean: the co-evolution of cyanobacterial metal requirements and biogeochemical cycles at the Archean–Proterozoic boundary? Inorg. Chim. Acta 356 (2003) 308–318.
[32] C. Vasconcelos, J.A. Mackenzie, Microbial mediation of modern dolomite precipitation and diagenesis under anoxic conditions (Lagoa Vermelha, Rio de janeiro, Brazil), J. Sediment. Res., Sect. A Sediment. Pet. Proc. 67 (1997) 378–390.
[33] Y. van Lith, R. Warthmann, C. Vasconcelos, J. McKenzie, Sulphate-reducing bacteria induce low-temperature Ca-dolomite and high Mg-calcite formation, Geobiology 1 (2003) 71–79.
[34] Y. Rosenthal, P. Lam, E.A. Boyle, J. Thomson, Authigenic cadmium enrichments in suboxic sediments: precipitation and postdepositional mobility, Earth Planet. Sci. Lett. 132 (1995) 99–111.
[35] S. Castanier, G. Le Métayer-Levrel, J.P. Perthuisot, Ca-carbonates precipitation and limestone genesis — the microbiogeologist point of view, Sediment. Geol. 126 (1999) 9–23.
[36] D.T. Wright, The role of sulphate-reducing bacteria and cyanobacteria in dolomite formation in distal ephemeral lakes of Coorong region, South Australia, Sediment. Geol. 126 (1999) 147–157.
[37] S.J. Mazullo, Organogenic dolomitization in peritidal to deep-sea sediments, J. Sediment. Res. 70 (2000) 10–23.
[38] G. Jiang, N. Christie-Blick, A.J. Kaufman, D.M. Banerjee, V. Rai, Carbonate platform growth and cyclicity at a terminal Proterozoic passive margin, Infra Krol Formation and Krol Group, Lesser Himalaya, India, Sedimentology 50 (2003) 921–952.
[39] F.A. Corsetti, A.J. Kaufman, Stratigraphic investigations of carbon isotope anomalies and Neoproterozoic ice ages in Death Valley, California, Geol. Soc. Amer. Bull. 115 (2003) 916–932.
[40] M.J. Kennedy, N. Christie-Blick, L.E. Sohl, Are Proterozoic cap carbonates and isotopic excursions a record of gas hydrate destabilization following Earth's coldest intervals? Geology 29 (2001) 443–446.
[41] Y. Shen, T. Zhang, X. Chu, C-isotopic stratification in a Neoproterozoic post-glacial ocean, Precambrian Res. 137 (2005) 243–251.
[42] J.P. Grotzinger, A.H. Knoll, Anomalous carbonate precipitates: is the Precambrian the keyto the Permian? Palaios 10 (1995) 578–596.
[43] D. Rothman, J.M. Hayes, R.E. Summons, Dynamics of the Neoproterozoic carbon cycle, PNAS 100–14 (2003) 8124–8129.